Cite This: J. Phys. Chem. A XXXX, XXX, XXX–XXX

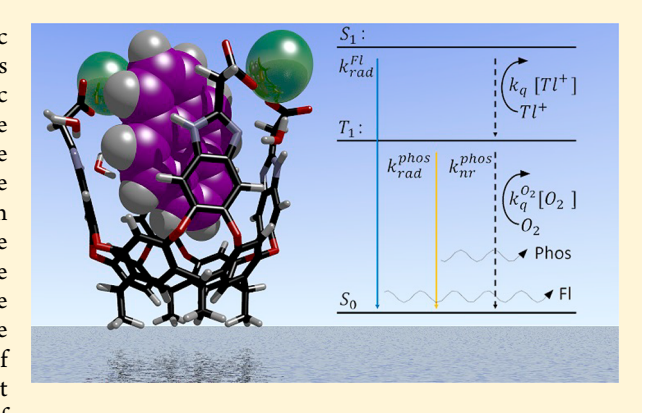
# Boosting the Heavy Atom Effect by Cavitand Encapsulation: Room Temperature Phosphorescence of Pyrene in the Presence of Oxygen

Connor J. Easley, Magi Mettry, Emily M. Moses, Richard J. Hooley,\* and Christopher J. Bardeen\*

Department of Chemistry, University of California—Riverside, Riverside, California 92521, United States

Supporting Information

**ABSTRACT:** A deep cavitand is used to encapsulate the aromatic molecule pyrene in its interior while also binding  $Tl^+$  ions with its terminal carboxylates. Steady-state and time-resolved spectroscopic experiments, along with quantum yield measurements, quantify the enhancements of intersystem crossing and room temperature phosphorescence due to cavitand encapsulation. These results are compared to those obtained for pyrene contained in sodium dodecyl sulfate micelles, which is the usual system used to generate room temperature phosphorescence. The combination of selective binding and strong  $Tl^+$  recognition by the cavitand enhances the intersystem crossing and decreases the phosphorescence radiative lifetime from  $\sim 30$  to 0.23 s. The cavitand also decreases the rate of  $O_2$  quenching by a factor of 100. Together, these factors can boost the room temperature phosphorescence signal by several orders of



magnitude, allowing it to be detected in water without  $O_2$  removal. Host:guest recognition provides a route to molecular-scale triplet emitters that can function under ambient conditions.

#### ■ INTRODUCTION

Triplet excited states in organic molecules play a central role in next-generation solar energy conversion schemes that rely on singlet fission and triplet-triplet annihilation upconversion. The detection of these states is typically accomplished using transient absorption methods, which have limited sensitivity compared to photoluminescence detection. For organic molecules, fluorescence from the excited singlet state S<sub>1</sub> to the ground singlet state S<sub>0</sub> is widely used for sensing and structural characterization. Phosphorescence from the triplet state T<sub>1</sub>, however, is formally spin-forbidden and typically not observed for organic molecules at room temperature. Research efforts are currently directed toward the design of systems that can show enhanced phosphorescence. Strategies to achieve efficient phosphorescence include the use of specialized solid matrices, 2-4 designing molecules with enhanced internal spinorbit coupling (SOC), 5-7 and designing molecules with small S<sub>1</sub>-T<sub>1</sub> energy gaps that exhibit thermally activated delayed fluorescence.

A general strategy to obtain phosphorescence without redesigning the organic molecule is to use the external heavy atom effect to induce SOC. The source of the heavy atom could be the solvent, e.g., methyl iodide, or it could be codissolved with the organic chromophore. If metal ion salts are used to enable SOC, then both species must be dissolved in water, and a surfactant is often used to bring the organic molecule into solution where it can encounter the heavy atom. The use of surfactants and heavy atom salts to induce SOC has led to the observation of room temperature phosphorescence

(RTP) in numerous polyaromatic hydrocarbons (PAHs). <sup>13–16</sup> However, surfactant concentrations greater than the critical micelle concentration (8 mM for sodium dodecyl sulfate (SDS)), high heavy atom salt concentrations, and strict deoxygenation are usually required, which have prevented RTP from being widely used.

In this article, we present a strategy for RTP that exploits noncovalent molecular recognition. A number of water-soluble hosts can bind hydrocarbons in water<sup>17–21</sup> and modify the guest photochemistry and photophysics.<sup>22–25</sup> If the host could also strongly bind heavy metal ions, both the PAH and the metal could be brought into close proximity, eliminating the need for excess surfactant and metal ions while optimizing the RTP output; the concept is outlined in Figure 1a. Deep cavitand 1 is capable of extracting hydrocarbons such as pyrene (PYR) into its cavity in water with an affinity  $K_a > 10^4 \text{ M}^{-1.26}$ and also binds heavy metal ions at the anionic periphery with an affinity  $K_1$   $(1 \cdot Pb^{2+}) = 7.5 \times 10^5 M^{-1.27}$  PYR is a PAH that exhibits RTP in the presence of heavy atoms, with Tl<sup>+</sup> being most commonly used. <sup>13,14,28–30</sup> The relevant energy levels and rate processes that determine the PYR phosphorescence output are outlined in Figure 1b. The goal of this paper is to assess the effects of encapsulation on these processes and determine whether it can increase the RTP output relative to the surfactant approach. We find that cavitand encapsulation can enhance the heavy atom SOC while protecting the

Received: June 19, 2018 Published: July 19, 2018 The Journal of Physical Chemistry A

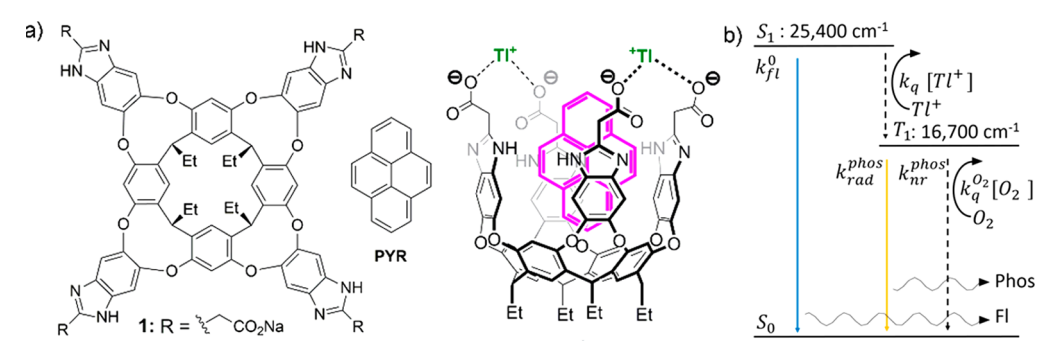


Figure 1. (a) Deep cavitand 1, pyrene (PYR) and a representation of the structure of the host:guest complex binding Tl<sup>+</sup> ions. (b) Jablonski diagram showing the electronic states and rates that are affected by cavitand encapsulation.

chromophore from  $\mathrm{O}_2$  quenching, leading to significant gains in RTP signal and making it observable even without degassing. These results suggest that it may be possible to design supramolecular complexes to light up molecular triplet states, which could then be used for sensing or detection.

#### EXPERIMENTAL SECTION

All solvents and TlNO3 were used as received from Sigma-Aldrich. Deep cavitand 1 was synthesized according to published procedures.<sup>26</sup> A [1] = 0.002 M solution was formed by mild sonication of 1 (1.7 mg, 0.0012 mmol) in H<sub>2</sub>O (0.6 mL) for 5 min. Solid PYR (5 mg) was powdered and added, and the resulting suspension sonicated for 24 h at room temperature. The suspension was filtered through a 0.2  $\mu$ m PTFE microfilter to remove solid pyrene that had not been extracted into the cavitand. The 1-PYR complex was prepared by sonicating the two molecules in water, removing the unencapsulated PYR by filtration and diluting to [1·PYR] = 6 μM. SDS-PYR solutions were made by stirring both species in water for 4 h. In the SDS-PYR samples, the concentration of PYR was also 6  $\mu$ M, and [SDS] = 20 mM to ensure micelle formation. All samples were prepared in Millipore deionized water and chemically degassed by adding  $Na_2SO_3 = 0.1$  M.

Steady-state absorption spectra were measured on a Cary 500 spectrophotometer. Steady-state fluorescence spectra were measured using a Horiba Scientific QM 400 fluorometer with a 2 nm band-pass. For emission spectra, the excitation wavelength was 337 nm and for excitation spectra the detection wavelength was 425 nm. All spectra were recorded using 1 cm path length quartz cuvettes. The thallium concentration was varied from  $[TI^+] = 0.00$  M to  $[TI^+] = 0.03$  M by adding a measured amount of TINO<sub>3</sub> stock solution to each sample.

To measure the RTP lifetimes, a 10 Hz, 337 nm nitrogen laser (Photochemical Research Associates, Inc. LN 1000 Nitrogen Laser) was used. The sample was excited and the RTP signal was directed through a 550 nm long wave pass filter in front of a photomultiplier tube connected to a digital oscilloscope (Tektronix TDS 3032B Digital Phosphor Oscilloscope). To measure nanosecond fluorescence lifetimes of the SDS-PYR samples, the sample was excited using 330 nm pulse derived from a Palitra optical parametric amplifier pumped by a 800 nm femtosecond pulse generated by a Coherent Libra Ti:sapphire laser system. The laser repetition rate was 1 kHz. The sample fluorescence was collected using front-face detection and focused into a Hamamatsu 3344 Streakscope streak camera.

## ■ RESULTS AND DISCUSSION

Figure 2 shows the absorption spectra of SDS-PYR and 1-PYR, along with those of PYR in cyclohexane and 1 in H<sub>2</sub>O for

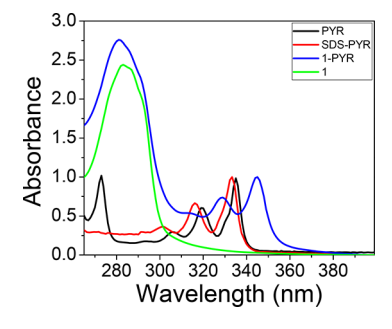
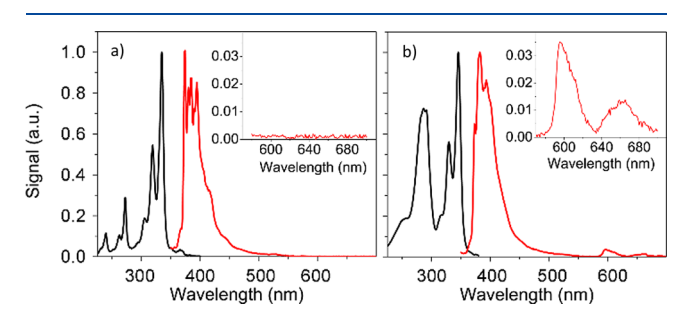


Figure 2. Absorbance spectra of pyrene in cyclohexane (black), SDS-PYR (red), 1·PYR (blue), and cavitand (green), all without thallium, are shown. They have been normalized to the highest peak of the pyrene absorption.

comparison. The general shape of the PYR absorbance, with well-resolved vibronic peaks, is preserved in all samples, suggesting that the environment does not strongly perturb the electronic structure. The PYR absorbance does shift to slightly shorter wavelengths in the aqueous SDS solution, presumably due to the presence of  $H_2O$  molecules that penetrate the micelles. The solvatochromic shift is much more pronounced for 1-PYR with a shift to lower energies consistent with a more polarizable environment inside the cavitand. The steady-state fluorescence excitation spectra for SDS-PYR and 1-PYR with  $[Tl^+] = 10$  mM, shown in Figure 3, closely resemble the absorption spectra. The SDS-PYR excitation has



**Figure 3.** Fluorescence excitation (black, detection wavelength = 425 nm) and emission (red, excitation wavelength = 337 nm) of (a) SDS-PYR and (b) 1·PYR. For each sample: [PYR] = 6  $\mu$ M and [TI<sup>+</sup>] = 10 mM and no degassing agent. The insets show the emission from 580 to 700 nm; RTP is present in 1·PYR, but not in SDS-PYR.

the same features as that of PYR, showing no electronic interaction between the SDS and PYR. The 1-PYR sample has an extra peak at 280 nm that corresponds to the main cavitand absorption peak in Figure 2. Its presence in the PYR excitation spectrum indicates that singlet energy transfer can occur from 1 to the PYR.

The spectra in Figures 2 and 3 indicate that the PYR environment inside the cavitand is significantly different from that in the micelles. The lowest energy absorption peak for 1. PYR is red-shifted to 345 nm, whereas that of the SDS-PYR occurs at 334 nm, indicating that the PYR experiences a polarizable environment in the cavitand. Additional evidence for the different environments can be obtained by analyzing the shape of the PYR fluorescence spectrum. The PYR fluorescence 0-0/0-2 vibronic peak ratio has been shown to be quite sensitive to the polarity of the local environment.<sup>33</sup> In the SDS-PYR spectrum, the ratio of peak heights is 1.2, roughly comparable to what is observed in methanol. This is most likely due to H2O molecules exchanging in and out of the loosely assembled micelle. The 1-PYR complex, however, exhibits a vibronic peak pattern in which the 0-0 peak is highly suppressed relative to the 0-2 peak, indicative of a nonpolar environment, roughly comparable to cyclohexane. All the steady-state spectral data are consistent with strong encapsulation of PYR in 1.

Perhaps the most interesting feature of the photoluminescence data is the existence of a small RTP peak at 598 nm for  $1 \cdot \text{PYR}$  in Figure 3b, even though the solution has not been degassed. No RTP could be detected from the SDS solution without chemical degassing. The presence of phosphorescence under ambient conditions provides an indication that the cavitand protects the PYR triplet state from  $O_2$  quenching, possibly by modifying the  $k_q^{O_2}$  rate. But since there are multiple processes involved in the generation of phosphorescence, it is important to quantify how cavitand encapsulation affects the different rates in Figure 1b in order to confirm this.

From Figure 1b, the phosphorescence yield will depend on several factors. The first step in generating phosphorescence involves intersystem crossing (ISC) from  $S_1$  to  $T_1$ , which will be enhanced in the presence of  $Tl^+$ . This rate can be inferred from the degree of  $S_1$  fluorescence quenching. To characterize how the  $Tl^+$  ions induce  $S_1 \rightarrow T_1$  ISC, we measured the dependence of the fluorescence and phosphorescence signals on  $[Tl^+]$ . The solutions are degassed by the addition of an  $O_2$  scavenger ( $[Na_2SO_3] = 0.1$  M) to isolate the effect of  $Tl^+$ . In the SDS-PYR samples, the integrated fluorescence (Figure 4a) signal decreases as  $[Tl^+]$  increases. We checked that this

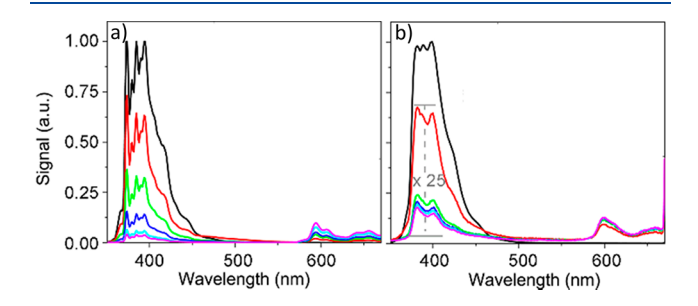


**Figure 4.** Fluorescence quenching of (a) SDS-PYR and (b) 1·PYR. Lines ( $[Tl^+]$  in mM): black, 0.0; red, 3.2; green, 9.1; blue, 14.3; light blue, 18.9; purple, 28.6. In (b), the spectra with  $[Tl^+]$  present have been multiplied by 25 to compare to the  $[Tl^+]$  = 0 mM spectrum.

decline in the steady-state signal was accompanied by a changing fluorescence lifetime (Supporting Information). This confirmed that the SDS-PYR quenching results from a dynamic process, presumably diffusive encounters between PYR and Tl<sup>+</sup> ions. The fluorescence signal of the 1·PYR declines even more rapidly as a function of [Tl<sup>+</sup>], as shown in Figure 4b. Attempts to measure the fluorescence lifetime changes of these samples were unsuccessful because the fluorescence emission of the 1·PYR samples with Tl<sup>+</sup> was too weak to be measured using the streak camera on the nanosecond time scale.

The fluorescence quenching data for SDS-PYR and 1·PYR are qualitatively different and will be analyzed using different models. For the SDS-PYR, we assume a dynamic quenching process with a rate given by  $k_{\rm q}[{\rm Tl}^+]$ . For this case, a standard Stern–Volmer analysis predicts that

$$\frac{I(0)}{I([Tl^+])} = 1 + \frac{k_q}{k_f^0} [Tl^+]$$
(1)

where I(0) is the fluorescence intensity without TI<sup>+</sup> present,  $I([TI^+])$  is the fluorescence intensity in the presence of TI<sup>+</sup>, and  $k_{\rm q}$  and  $k_{\rm fl}^0$  are defined in Figure 1b. We used the steady-state data to calculate  $k_{\rm q}$  because this experiment was repeated and had less uncertainty in the concentrations. The Stern–Volmer plot in Figure 5a yields  $k_{\rm q}=7\pm1\times10^9~{\rm M}^{-1}~{\rm s}^{-1}$  with

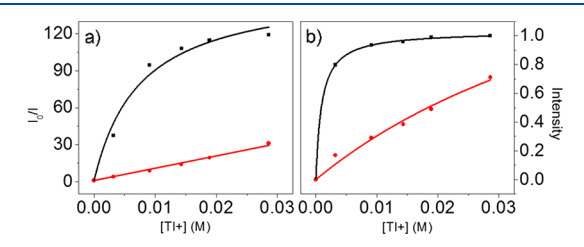


Figure 5. (a) Stern–Volmer plot of fluorescence quenching vs [Tl<sup>+</sup>] for SDS-PYR (black circles) and 1·PYR (red squares) along with fits to the models described in the Supporting Information. (b) Plot of RTP signal versus [Tl<sup>+</sup>] for SDS-PYR (black circles) and 1·PYR (red squares) along with fits to the models described in the Supporting Information.

 $k_{\rm fl}^0=6.5\times 10^6~{\rm s}^{-1}$  as measured in a separate experiment (Supporting Information). This value of  $k_{\rm q}$  is consistent with diffusion limited quenching of singlet states. <sup>34</sup>

In contrast to the SDS-PYR data, a plot of the  $1 \cdot PYR$  steady-state data shows a more rapid rise in the fluorescence quenching, followed by a leveling off after  $[Tl^+] = 0.01$  M (Figure 5a). This nonlinear behavior cannot be described using the Stern–Volmer model. Instead, we use a static quenching model that assumes that the  $Tl^+$  interaction with  $1 \cdot PYR$  obeys an association equilibrium constant. We can write the association reaction

$$\mathbf{1} \cdot \text{PYR} + \text{TI}^{+} \to \mathbf{1} \cdot \text{PYR}(\text{TI}^{+}) \qquad K_{\text{assoc}}^{\text{q}} = \frac{[\mathbf{1} \cdot \text{PYR}(\text{TI}^{+})]}{[\mathbf{1} \cdot \text{PYR}][\text{TI}^{+}]}$$
(2

This model allows us to fit the data in terms of the equilibrium constant for the quenching reaction  $K_{\rm assocc}^{\rm q}$  and  $P_{\rm quench}$ , the probability that a Tl<sup>+</sup> ion quenches the fluorescence after binding (Supporting Information). The equation for integrated fluorescence intensity is given by

$$\frac{I(0)}{I([Tl^+])} = \frac{1 + K_{assoc}^{q}[Tl^+]}{1 + (1 - P_{quench})K_{assoc}^{q}[Tl^+]}$$
(3)

The parameters  $P_{\rm quench}$  and  $K_{\rm assoc}^{\rm q}$  were varied to fit the data in Figure 5a, and the results are overlaid with the data. We find  $K_{\rm assoc}^{\rm q} = 2.1 \pm 0.4 \times 10^4 \ {\rm M}^{-1}$  and  $P_{\rm quench} = 0.994$ . The Tl<sup>+</sup> ions that promote the S<sub>1</sub>  $\rightarrow$  T<sub>1</sub> ISC process should

The  $Tl^+$  ions that promote the  $S_1 \rightarrow T_1$  ISC process should also enhance the phosphorescence transition  $(T_1 \rightarrow S_0)$ . The photoluminescence spectra in Figure 4 allow us to plot the growth of the RTP signal as a function of  $[Tl^+]$ , as shown in Figure 5b. The SDS-PYR RTP shows an apparent linear increase in signal. Application of the Stern–Volmer model to the growth of the phosphorescence signal leads to a more complex expression that is derived in the Supporting Information. Here we only give the final result,

$$Phos([Tl^{+}]) \propto \frac{k_{e}N_{S1}(0)[Tl^{+}]k_{SO}[Tl^{+}]}{(k_{trip} + k_{SO}[Tl^{+}])(k_{fl}^{0} + k_{q}[Tl^{+}])}$$
(4)

In this equation, the parameters are the  $S_1$  population decay  $(k_{\rm fl}^0)$ , the rate of intersystem crossing due to thallium  $(k_{\rm q})$ , the intrinsic decay rate of the  ${\rm T_1}$  state  $(k_{\rm trip})$ , and the rate of spinorbit coupling  $(k_{\rm SO})$  that leads to enhanced phosphorescence from the  ${\rm T_1}$  state.  $k_{\rm q}=7\pm1\times10^9~{\rm M^{-1}~s^{-1}}$  with  $k_{\rm fl}^0=6.5\times10^6~{\rm s^{-1}}$  are fixed by our previous results, while  $k_{\rm trip}=87~{\rm s^{-1}}$  was measured as described below. The curve in Figure 5b can be fit using a scaling prefactor and with the ratio  $\frac{k_{\rm SO}}{k_{\rm trip}}=22~{\rm M^{-1}}$ . This

fit leads to a quasi-linear increase in the RTP signal with  $[Tl^+]$  because the  $k_q[Tl^+]$  term in the denominator is dominant.

The growth of RTP for 1-PYR is again nonlinear but can be analyzed using an equilibrium model similar to that given in eq 1. We assume that the Tl<sup>+</sup> ions that promote phosphorescence obey an equilibrium similar to those that promote ISC, but with a different equilibrium constant in eq 2, which we denote  $K_{\rm assoc}^{\rm RTP}$  instead of  $K_{\rm assoc}^{\rm q}$ . We derive an expression for the phosphorescence signal (Supporting Information),

$$Phos([Tl^{+}]) \propto K_{assoc}^{RTP}[\mathbf{1} \cdot PYR][Tl^{+}] = \frac{[\mathbf{1} \cdot PYR]_{0} K_{assoc}^{RTP}[Tl^{+}]}{1 + K_{assoc}^{RTP}[Tl^{+}]}$$
(5)

From a plot of phosphorescence versus thallium concentration,  $K_{\text{assoc}}^{\text{RTP}}$  can be determined to be  $1.1 \pm 0.1 \times 10^3 \text{ M}^{-1}$ . The  $K_{\text{assoc}}^{\text{RTP}}$  found by this analysis is 20× smaller than  $K_{\text{assoc}}^{\text{q}}$  the association constant for fluorescence quenching. Attempts to fit the different curves using a single association constant were unsuccessful (Supporting Information). The different values for  $K_{\text{assoc}}^{\text{q}}$  and  $K_{\text{assoc}}^{\text{RTP}}$  suggest that fluorescence quenching and RTP have different sensitivities to the Tl+ binding. This may not be too surprising in light of the fact that (a) the  $S_1 \rightarrow T_1$ and  $T_1 \rightarrow S_0$  transitions involve different electronic states and (b) the four carboxylate groups in 1 can complex a variable number of ions. 27,35 For example, it is possible that a single Tl+ ion suffices to induce ISC from  $S_1$  to  $T_1$ , but two ions, or binding to a different site, is required to enhance the RTP from  $T_1$  to  $S_0$ . A more sophisticated model that considers Poissonian binding statistics<sup>36–38</sup> and different SOC terms for different electronic states is probably needed to quantitatively describe the dependence of both ISC and RTP on [Tl<sup>+</sup>]. The important point is that the concentration dependence of the fluorescence quenching and RTP enhancement for 1-PYR are both consistent with equilibrium binding of the Tl<sup>+</sup> ions.

Once the  $T_1$  state is populated, the next question is how the differences in PYR binding and  $Tl^+$  association affect the absolute quantum yield  $QY_{phos}$ . This quantity is determined by the ratio of the phosphorescence radiative rate  $k_{rad}^{phos} = \frac{1}{\tau_{phos}^{phos}}$  to

the total triplet decay rate  $k_{\text{tot}}^{\text{phos}} = \frac{1}{\tau_{\text{phos}}}$ . From eq 4, we can identify  $k_{\text{rad}}^{\text{phos}} \cong k_{\text{SO}}[\text{Tl}^+]$  if the radiative rate is dominated by the heavy atom induced SOC.

 $k_{\rm tot}^{\rm phos}$  is the sum of all rates that depopulate T<sub>1</sub>. These include  $k_{\rm rad}^{\rm phos}$ , the O<sub>2</sub> quenching rate given by  $k_{\rm q}^{\rm O_2}[{\rm O_2}]$ , and any other nonradiative pathways resulting from encapsulation, which are contained in  $k_{\rm nr}^{\rm phos}$ . It also includes the intrinsic triplet decay time in the absence of Tl<sup>+</sup>,  $k_{\rm trip}$ .

$$QY_{\text{phos}} = \frac{k_{\text{rad}}^{\text{phos}}}{k_{\text{tot}}^{\text{phos}}} = \frac{k_{\text{rad}}^{\text{phos}}}{k_{\text{trip}} + k_{\text{rad}}^{\text{phos}} + k_{\text{nr}}^{\text{phos}} + k_{\text{q}}^{O_2}[O_2]}$$
(6)

In principle, the host:guest binding can affect all these quantities, but we focus on changes in  $k_{\rm rad}^{\rm phos}$  (via improved SOC due to the bound Tl<sup>+</sup>) and  $k_{\rm q}^{\rm Q}$  (via protection of the T<sub>1</sub> state by the cavitand). For a SDS-PYR sample degassed with Na<sub>2</sub>SO<sub>3</sub> and with [Tl<sup>+</sup>] = 0.01 M, we measured QY<sub>phos</sub>(SDS) = 0.003  $\pm$  0.001, using anthracene as a standard (Supporting Information). The lifetime of the RTP is  $\tau_{\rm phos}({\rm SDS})$  = 11.5 ms (Figure 6a), in good agreement with the PYR triplet lifetime in

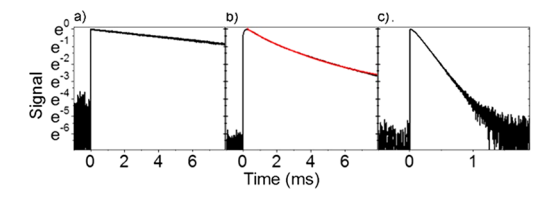


Figure 6. Phosphorescence decays for (a) SDS-PYR without oxygen, (b) 1-PYR without oxygen (red line: stretched exponential fit), and (c) 1-PYR with oxygen. Note the different time axis in (c). The lifetimes of each are 11.5, 1.61, and 0.206 ms, respectively.

neat liquids and micelles. <sup>34,39</sup> Combining these two measurements allows us to estimate the phosphorescence radiative lifetime  $t_{\rm rad}^{\rm phos}({\rm SDS}) = \frac{\tau_{\rm phos}}{{\rm QY}_{\rm phos}} = 3.8 \pm 1.0$  s. The radiative

lifetime for free, uncomplexed PYR lies in the range 30–60 s. 40,41 For SDS-PYR, [Tl+] = 0.01 M enhances the radiative rate by roughly a factor of 10, presumably through SOC interactions averaged over random ion–molecule configurations

For the same [Tl<sup>+</sup>], the 1-PYR system has  $QY_{phos}(1) = 0.007 \pm 0.002$ . Unfortunately, the RTP decay of this sample is not a simple exponential. The RTP signal in Figure 6b shows a period of initial growth spanning several hundred microseconds, followed by a nonexponential decay which is initially more rapid than that of SDS-PYR. The initial growth is too slow to be singlet energy transfer from 1 to PYR but could reflect triplet energy transfer from 1 that absorbs the 337 nm excitation via weak  $n \to \pi^*$  transitions. The nonexponential RTP decay of the 1-PYR complex may reflect heterogeneity in the Tl<sup>+</sup> binding and  $k_{nr}^{phos}$ . The region of the decay after 1 ms can be fit using a stretched exponential of the form

$$\exp\left[-\left(\frac{t}{\tau_{\text{phos}}}\right)^{\alpha}\right]$$
 with  $\tau_{\text{phos}} = 1.61$  ms and the exponent  $\alpha = 1.61$ 

0.78. If we take  $\tau_{\rm phos}$  to be the average lifetime, we can estimate

an average radiative lifetime  $\tau_{\rm rad}^{\rm phos}$  (1) = 0.23 s, roughly 10× less than that measured for the SDS-PYR micelles. This shorter radiative lifetime may reflect the closer positioning of Tl<sup>+</sup> ions to PYR by the cavitand carboxylates, as SOC has been shown to be sensitive to the spatial location of the heavy atom. <sup>42,43</sup> Alternatively, it may be that the cavitand simply keeps the Tl<sup>+</sup> ions in proximity with PYR for a longer time, and the time-averaged interaction is greater than in micelles, where both ion and molecule are diffusing.

Finally, we turn to the last important rate process that controls the RTP magnitude, quenching of the  $T_1$  state by  $O_2$ . Under ambient conditions,  $[O_2] = 2.7 \times 10^{-4}$  M in water, while the  $O_2$  triplet quenching constant  $k_q^{O_2}$  is  $\sim 2 \times 10^9$  s<sup>-1</sup> M<sup>-1</sup> in neat liquids.<sup>34</sup> If we assume that the micelle behaves like a neat liquid and does not significantly impede  $O_2$  diffusion, then these values lead to an estimated triplet lifetime of 1.8  $\mu$ s in the presence of  $O_2$ . Given a 3.8 s radiative lifetime, the effective quantum yield is less than  $10^{-6}$ , explaining why RTP for the micelle system is not observable with  $O_2$  present. The 1-PYR complex, however, has a measured RTP lifetime of  $206 \pm 15 \ \mu$ s (Figure 6c) in the presence of  $O_2$ . If we assume that this lifetime is dominated by  $O_2$  quenching, then  $k_q^{O_2}[O_2] = 1/206 \ \mu$ s, which allows us to estimate a value  $k_q^{O_2} = 1.7 \times 10^7$  s<sup>-1</sup> M<sup>-1</sup> for 1-PYR (Supporting Information), which is  $100 \times$  smaller than for PYR in neat organic liquids.

Similar levels of O2 protection have been observed for PYR and other molecules in an octa acid cavitand, 44,45 although O2 has also been shown to penetrate this same cavitand for other guest molecules. 46 Protection from O2 quenching has also been observed for cyclodextrin and cucurbituril encapsulation. 47,48 For 1, we believe that the long residence time of PYR prevents O2 access to the aromatic core. PYR rotates inside 1's cavity rapidly on the NMR time scale but has a slow in/out exchange rate of  $\sim 10 \text{ s}^{-1.26}$  When the 1-PYR arms are closed, modeling illustrates that O<sub>2</sub> molecules can only access the upper edges of the aromatic ring (Supporting Information, Figure S-2), rather than the  $\pi$  cloud. The molecular geometry of the  $O_2$  triplet quenching interaction is not known, but O2 is believed to preferentially interact with the  $\pi$  face of PAHs, making a weakly bound charge-transfer complex. This complex is a likely intermediate in the T<sub>1</sub> quenching process.<sup>49</sup> We hypothesize that the host protects the T<sub>1</sub> state by preventing access to the  $\pi$ -system of PYR, even though the system remains fluid and the PYR is not strongly perturbed.

With the effects of encapsulation and Tl+ association measured, we can now quantitatively assess how using the cavitand affects the RTP output. In the absence of O2, the  $QY_{phos}$  of 1.PYR is ~2× larger than that of SDS-PYR. Although 1.PYR is more effective at complexing Tl<sup>+</sup> and has a  $k_{\rm rad}^{\rm phos}$  value that is 10× higher, these advantages are partially canceled out by an increase in  $k_{\rm nr}^{\rm phos}$  that shortens the overall phosphorescence lifetime. However, there is a long-lived component of the RTP decay (Figure 6b), suggesting some of the 1-PYR molecules do not experience more rapid nonradiative relaxation. It may be possible to reap the full benefit of the increased  $k_{\rm rad}^{\rm phos}$  if the heterogeneity could be eliminated and increased  $k_{\rm nr}^{\rm phos}$  values could be avoided. The real advantage of the cavitand becomes apparent when O2 is present. For nondegassed aqueous solutions, the cavitand boosts the  $QY_{phos}$  by a factor of 100 by reducing  $k_q^{O_2}$ . In the ideal case, with complete conversion to  $T_1$  by ISC and elimination of those geometries that give rise to accelerated nonradiative relaxation, our results suggest that an overall improvement in QY<sub>phos</sub> on

the order of 1000 should be possible by using cavitand encapsulation. It is possible that optimization of cavitand structure and choosing a guest molecule with a larger intrinsic  $k_{\rm rad}^{\rm phos}$  could boost the enhancement factor even further.

The results of this paper demonstrate that the combination of selective PAH binding and strong Tl<sup>+</sup> recognition by a deep cavitand host can lead to enhanced intersystem crossing and phosphorescence radiative rates. Meanwhile, the confined cavitand geometry can protect the guest triplet state from O<sub>2</sub> quenching interactions. Together, these factors boost the RTP signal of PYR by several orders of magnitude, allowing its detection in room temperature water in the presence of oxygen. Host:guest recognition may provide a promising route toward creating self-contained, molecular-scale triplet emitters.

#### ASSOCIATED CONTENT

## Supporting Information

The Supporting Information is available free of charge on the ACS Publications website at DOI: 10.1021/acs.jpca.8b05813.

<sup>1</sup>H NMR spectra, minimized structural models, photoluminescence measurements and fluorescence decays, measurements of rate constants for fluorescence quenching, measurements of RTP growth, curve fitting for concentrationd dependent data and Stern–Volmer plot, quantum yield measurement and emission spectra, exponential fitting of RTP decay and time decay curve, quenching constant determination (PDF)

#### AUTHOR INFORMATION

## **Corresponding Authors**

\*R. J. Hooley. E-mail: richard.hooley@ucr.edu.

\*C. J. Bardeen. E-mail: christopher.bardeen@ucr.edu.

#### ORCID ®

Christopher J. Bardeen: 0000-0002-5755-9476

#### Notes

The authors declare no competing financial interest.

## ACKNOWLEDGMENTS

The authors thank the National Science Foundation (DMR-1508099 to C.J.B. and CHE-1708019 to R.J.H.) for support. We acknowledge the National Science Foundation grant CHE-1626673 for the purchase of a Bruker Avance Neo 400 spectrometer.

## **■** REFERENCES

- (1) Lakowicz, J. R. Principles of Fluorescence Spectroscopy; Kluwer: New York, 1999.
- (2) Gurney, R. W.; Mitchell, C. A.; Ham, S.; Bastin, L. D.; Kahr, B. Salting Benzenes. *J. Phys. Chem. B* **2000**, *104*, 878–892.
- (3) Hirata, S.; Totani, K.; Zhang, J.; Yamashita, T.; Kaji, H.; Marder, S. R.; Watanabe, T.; Adachi, C. Efficient Persistent Room Temperature Phosphorescence in Organic Amorphous Materials under Ambient Conditions. *Adv. Funct. Mater.* **2013**, *23*, 3386–3397.
- (4) Reineke, S.; Seidler, N.; Yost, S. R.; Prins, F.; Tisdale, W. A.; Baldo, M. A. Highly Efficient, Dual State Emission from an Organic Semiconductor. *Appl. Phys. Lett.* **2013**, *103*, 093302.
- (5) Baldo, M. A.; O'Brien, D. F.; You, Y.; Shoustikov, A.; Sibley, S.; Thompson, M. E.; Forrest, S. R. Highly Efficient Phosphorescent Emission from Organic Electroluminescent Devices. *Nature* **1998**, 395, 151–154.
- (6) Adachi, C.; Baldo, M. A.; Thompson, M. E.; Forrest, S. R. Nearly 100% Internal Phosphorescence Efficiency in an Organic Light-Emitting Device. *J. Appl. Phys.* **2001**, *90*, 5048–5051.

The Journal of Physical Chemistry A

- (7) Chaudhuri, D.; Sigmund, E.; Meyer, A.; Rock, L.; Klemm, Philippe; Lautenschlager, S.; Schmid, A.; Yost, S. R.; Voorhis, T. V.; Bange, S.; Hoger, S.; Lupton, J. M. Metal-Free OLED Triplet Emitters by Side-Stepping Kasha's Rule. *Angew. Chem., Int. Ed.* **2013**, *52*, 13449–13452.
- (8) Uoyama, H.; Goushi, K.; Shizu, K.; Nomura, H.; Adachi, C. Highly Efficient Organic Light- Emitting Diodes from Delayed Fluorescence. *Nature* **2012**, *492*, 234–238.
- (9) Yang, Z.; Mao, Z.; Xie, Z.; Zhang, Y.; Liu, S.; Zhao, J.; Xu, J.; Chi, Z.; Aldred, M. P. Recent Advances in Organic Thermally Activated Delayed Fluorescence Materials. *Chem. Soc. Rev.* **2017**, 46, 915–1016.
- (10) McGlynn, S. P.; Azumi, T.; Kasha, M. External heavy atom spin-orbital coupling effect. V. Absorption studies of triplet states. *J. Chem. Phys.* **1964**, *40*, 507–515.
- (11) Ramamurthy, V.; Caspar, J. V.; Eaton, D. F.; Kuo, E. W.; Corbin, D. R. Heavy-Atom-Induced Phosphorescence of Aromatics and Olefins Included within Zeolites. *J. Am. Chem. Soc.* **1992**, *114*, 3882–3892.
- (12) Bolton, O.; Lee, K.; Kim, H.-J.; Lin, K. Y.; Kim, J. Activating Efficient Phosphorescence from Purely Organic Materials by Crystal Design. *Nat. Chem.* **2011**, *3*, 205–210.
- (13) Kalyanasundaram, K.; Grieser, F.; Thomas, J. K. Room Temperature Phosphorescence of Aromatic Hydrocarbons in Aqueous Micellar Solutions. *Chem. Phys. Lett.* **1977**, *51*, 501–505.
- (14) Love, L. J. C.; Skrilec, M.; Habarta, J. G. Analysis by Micelle-Stabilized Room Temperature Phosphorescence in Solution. *Anal. Chem.* **1980**, *52*, 754–759.
- (15) Woods, R.; Love, L. J. C. Heavy Atom and Complexation Effects on Micelle Stabilized Room Temperature Phosphorescence of Anthracene, Acridine and Phenazine. *Spectrochim. Acta, Part A* **1984**, 40, 643–650.
- (16) Kuijt, J.; Ariese, F.; Brinkman, U. A. T.; Gooijer, C. Room Temperature Phosphorescence in the Liquid State as a Tool in Analytical Chemistry. *Anal. Chim. Acta* **2003**, *488*, 135–171.
- (17) Rekharsky, M. V.; Inoue, Y. Complexation Thermodynamics of Cyclodextrins. *Chem. Rev.* **1998**, *98*, 1875–1917.
- (18) Barrow, S. J.; Kasera, S.; Rowland, M. J.; del Barrio, J.; Scherman, O. A. Cucurbituril-Based Molecular Recognition. *Chem. Rev.* **2015**, *115*, 12320–12406.
- (19) Biros, S. M.; Rebek, J., Jr. Structure and Binding Properties of Water-Soluble Cavitands and Capsules. *Chem. Soc. Rev.* **2007**, *36*, 93–104
- (20) Laughrey, Z.; Gibb, B. C. Water-Soluble, Self-Assembling Container Molecules: an Update. *Chem. Soc. Rev.* **2011**, *40*, 363–386.
- (21) Lu, X.; Isaacs, L. Uptake of Hydrocarbons in Aqueous Solution by Encapsulation inAcyclic Cucurbit[n]uril-Type Molecular Containers. *Angew. Chem., Int. Ed.* **2016**, *55*, 8076–8080.
- (22) Kaanumalle, L. S.; Gibb, C. L. D.; Gibb, B. C.; Ramamurthy, V. Controlling Photochemistry with Distinct Hydrophobic Nanoenvironments. *J. Am. Chem. Soc.* **2004**, *126*, 14366–14367.
- (23) Berryman, O. B.; Dube, H.; Rebek, J. Photophysics Applied to Cavitands and Capsules. *Isr. J. Chem.* **2011**, *51*, 700–709.
- (24) Ramamurthy, V.; Sivaguru, J. Supramolecular Photochemistry as a Potential Synthetic Tool: Photocycloaddition. *Chem. Rev.* **2016**, 116, 9914–9993.
- (25) Murray, J.; Kim, K.; Ogoshi, T.; Yao, W.; Gibb, B. C. The Aqueous Supramolecular Chemistry of Cucurbit[n]urils, Pillar[n]-arenes and Deep-Cavity Cavitands. *Chem. Soc. Rev.* **2017**, *46*, 2479–2496.
- (26) Hooley, R. J.; van Anda, H. J.; Rebek, J. Extraction of Hydrophobic Species into a Water-Soluble Synthetic Receptor. *J. Am. Chem. Soc.* **2007**, *129*, 13464–13473.
- (27) Liu, Y.; Mettry, M.; Gill, A. D.; Perez, L.; Zhong, W.; Hooley, R. J. Selective Heavy Element Sensing with a Simple Host-Guest Fluorescent Array. *Anal. Chem.* **2017**, *89*, 11113–11121.
- (28) Ramos, G. R.; Khasawneh, I. M.; Garcia-Alvarez-Coque, M. C.; Winefordner, J. D. Room-Temperature Phosphorimetry of Polyar-

- omatic Hydrocarbons with Organized Media and Paper Substrate: A Comparative Study. *Talanta* 1988, 35, 41–46.
- (29) Kim, H.; Crouch, S. R.; Zabik, M. J.; Selim, S. A. Environmental Factors Affecting Micellar Stabilized Room-Temperature Phosphorescence Lifetimes. *Anal. Chem.* **1990**, *62*, 2365–2369.
- (30) Li, L.; Zhang, Z.; Long, W.; Tong, A. Study of Properties on Non-Protected Room Temperature Phosphorescence and Delayed Excimer Fluorescence of Pyrene Solution. *Spectrochim. Acta, Part A* **2001**, *57*, 385–393.
- (31) Martens, F. M.; Verhoeven, J. W. Charge-Transfer Complexation in Micellar Solutions. Water Penetrability of Micelles. *J. Phys. Chem.* **1981**, *85*, 1773–1777.
- (32) Melo, E. C. C.; Costa, S. M. B.; Maçanta, A. L.; Santos, H. The use of the n-(9-anthroyloxy) stearic acid to probe the water content of sodium dodecyl sulfate, dodecyltimethylammonium chloride, and triton X-100 micelles. *J. Colloid Interface Sci.* **1991**, *141*, 439–453.
- (33) Nakajima, A. Solvent Effect on the Vibrational Structures of the Fluorescence and Absorption Spectra of Pyrene. *Bull. Chem. Soc. Jpn.* **1971**, *44*, 3272–3277.
- (34) Murov, S. L.; Carmichael, I.; Hug, G. L. Handbook of Photochemistry; Marcel Dekker: New York, 1993.
- (35) Tang, H.; Fuentealba, D.; Ko, Y. H.; Selvapalam, N.; Kim, K.; Bohne, C. Guest Binding Dynamics with Cucurbit[7]uril in the Presence of Cations. *J. Am. Chem. Soc.* **2011**, *133*, 20623–20633.
- (36) Koole, R.; Luigjes, B.; Tachiya, M.; Pool, R.; Vlugt, T. J. H.; Donega, C. d. M.; Meijerink, A.; Vanmaekelbergh, D. Differences in Cross-Linnk Chemistry between Rigid and Flexible Dithiol Molecules Revealed by Optical Studies of CdTe Quantum Dots. *J. Phys. Chem. C* **2007**, *111*, 11208–11215.
- (37) Snee, P. T.; Tyrakowski, C. M.; Page, L. E.; Isovic, A.; Jawid, A. M. Quantifying Quantum Dots through Forser Resonant Energy Transfer. *J. Phys. Chem. C* **2011**, *115*, 19578–19582.
- (38) Li, X.; Nichols, V. M.; Zhou, D.; Lim, C.; Pau, G. S. H.; Bardeen, C. J.; Tang, M. L. Observation of Multiple, Identical Binding Sites in the Exchange of Carboxylic Acid Ligands with CdS Nanocrystals. *Nano Lett.* **2014**, *14*, 3382–3387.
- (39) Yansheng, W.; Weijun, J.; Changsong, L.; Huiping, Z.; Hongbo, T.; Naichang, Z. Study on Micelle Stabilized Room Temperature Phosphorescence Behavior of Pyrene by Laser Induced Time Resolved Technique. *Spectrochim. Acta, Part A* 1997, 53, 1405–1410.
- (40) Kropp, J. L.; Dawson, W. R.; Windsor, M. W. Radiative and Radiationless Processes in Aromatic Molecules. Pyrene. *J. Phys. Chem.* **1969**, 73, 1747–1752.
- (41) Langelaar, J.; Rettschnick, R. P. H.; Hoijtink, G. J. Studies on Triplet Radiative Lifetimes, Phosphorescence, and Delayed Fluorescence Yields of Aromatic Hydrocarbons in Liquid Solutions. *J. Chem. Phys.* **1971**, *54*, 1–7.
- (42) Ghosh, S.; Petrin, M.; Maki, A. H. Dependence of the Triplet State Properties on the Orientation of Metal Ion Perturbers in Naphthalene-Crown Ether Metal Ion Complexes. I. External Heavy Atom Effect. J. Chem. Phys. 1987, 87, 4315–4323.
- (43) Kundu, N.; Audhya, A.; Abtab, S. M. T.; Ghosh, S.; Tiekink, E. R. T.; Chaudhury, M. Anion-Controlled Assembly of Silver(I) Complexes of Multiring Heterocyclic Ligands: A Structural and Photophysical Study. *Cryst. Growth Des.* **2010**, *10*, 1269–1282.
- (44) Jayaraj, N.; Maddipatla, M. V. S. N.; Prabhakar, R.; Jockusch, S.; Turro, N. J.; Ramamurthy, V. Closed Nanocontainer Enables Thioketones to Phosphoresce at Room Temperature in Aqueous Solution. *J. Phys. Chem. B* **2010**, *114*, 14320–14328.
- (45) Jayaraj, N.; Jockusch, S.; Kaanumalle, L. S.; Turro, N. J.; Ramamurthy, V. Dynamics of Capsuleplex Formed Between Octaacid and Organic Guest Molecules Photophysical Techniques Reveal the Opening and Closing of Capsuleplex. *Can. J. Chem.* **2011**, *89*, 203–213.
- (46) Natarajan, A.; Kaanumalle, L. S.; Jockusch, S.; Gibb, C. L. D.; Gibb, B. C.; Turro, N. J.; Ramamurthy, V. Controlling Photoreactions with Restricted Spaces and Weak Intermolecular Forces: Exquisite Selectivity during Oxidation of Olefins by Singlet Oxygen. *J. Am. Chem. Soc.* **2007**, *129*, 4132–4133.

The Journal of Physical Chemistry A

- (47) Ponce, A.; Wong, P. A.; Way, J. J.; Nocera, D. G. Intense Phosphorescence Triggered by Alcohols upon Formation of a Cyclodextrin Ternary Complex. *J. Phys. Chem.* **1993**, *97*, 11137–11142.
- (48) Gonzalez-Bejar, M.; Montes-Navajas, P.; Garcia, H.; Scaiano, J. C. Methylene Blue Encapsulation in Cucurbit[7]uril: Laser Flash Photolysis and Near-IR Luminescence Studies of the Interaction with Oxygen. *Langmuir* **2009**, *25*, 10490–10494.
- (49) Paterson, M. J.; Christiansen, O.; Jensen, F.; Ogilby, P. R. Overview of Theoretical and Computational Methods Applied to the Oxygen-Organic Molecule Photosystem. *Photochem. Photobiol.* **2006**, 82, 1136–1160.